Journal of Power Sources 196 (2011) 1156–1162

Contents lists available at ScienceDirect

Journal of Power Sources

journal homepage: www.elsevier.com/locate/jpowsour

A high performance ceria based interdiffusion barrier layer prepared by spin-coating

Pawel Plonczak [a], Mario Joost [b], Johan Hjelm [a], Martin Søgaard [a,*], Mats Lundberg [a], Peter Vang Hendriksen [a]

[a] Fuel Cell and Solid State Chemistry Division, Risø National Laboratory – DTU, Frederiksborgvej 399, DK-4000 Roskilde, Denmark
[b] Institut fur Anorganische und Analytische Chemie, Corrensstr. 28/30, D-48149 Münster, Germany

ARTICLE INFO

Article history:
Received 30 June 2010
Received in revised form 13 August 2010
Accepted 30 August 2010
Available online 9 September 2010

Keywords:
Barrier layer
Spin-coating
SOFC
CGO
Thin film

ABSTRACT

A multiple spin-coating deposition procedure of $Ce_{0.9}Gd_{0.1}O_{1.95}$ (CGO) for application in solid oxide fuel cells (SOFCs) was developed. The thin and dense CGO layer can be employed as a barrier layer between yttria stabilised zirconia (YSZ) electrolyte and a (La, Sr)(Co, Fe)O_3 based cathode. The decomposition of the polymer precursor used in the spin-coating process was studied. The depositions were performed on anode supported half cells. By controlling the sintering temperature between each spin-coating process, dense and crack-free CGO films with a thickness of approximately 1 μm were obtained. The successive steps of dense layer production was investigated by scanning electron microscopy. X-ray diffraction was employed to monitor the crystal structure of the CGO layer sintered at different temperatures. The described spin coated barrier layer was evaluated using an anode supported cell with a composite cathode made of $La_{0.58}Sr_{0.4}Co_{0.2}Fe_{0.8}O_3$ (LSCF) and $Ce_{0.9}Gd_{0.1}O_{1.95}$. The developed CGO layer, was sufficient to restrain reactions between the perovskite based electrode and the electrolyte.

1. Introduction

In order to increase the efficiency of solid oxide fuel cells (SOFCs) especially at low temperatures it is necessary to reduce the cathode polarisation [1]. Replacing the commonly used (La, Sr)MnO_3 cathode material by electro-catalysts containing iron and cobalt in the B-sublattice such as (La,Sr)(Co,Fe)O_3 can significantly reduce the polarisation. However, at high temperature LSCF-based perovskites react with the standard yttria stabilised zirconia (YSZ) electrolyte forming $La_2Zr_2O_7$ and $SrZrO_3$ [2,3]. The oxide-ion conductivity of these reaction products are 3.7×10^{-6} and 4.3×10^{-5} S cm^{-1} at 750 °C for $La_2Zr_2O_7$ and $SrZrO_3$, respectively [4], which is low compared with the conductivity of pure 8YSZ (approximately 0.01 S cm^{-1} [5]). Thus the formation of these rection products significantly reduce cell performance. One solution to this problem is to employ an interdiffusion barrier layer between a LSCF-based cathode and the YSZ electrolyte [6,7]. $Ce_{0.9}Gd_{0.1}O_{1.95}$ (CGO) is usually used as barrier layer as it has a high oxide ion conductivity, inertness towards both LSCF and YSZ (at low temperatures) as well as chemical stability under cell operating conditions. An ideal interdiffusion barrier should be thin (with respect to the electrolyte thickness), of as high volumetric density as possible, and should allow manufacturing by a fast, cost-efficient, and up-scalable process.

Conventional ceramic thick film deposition techniques such as screen printing or spraying followed by constrained sintering, or co-firing with the half-cell, generally require temperatures above 1200 °C in order to generate sufficient densification and adhesion of the CGO layer to the electrolyte. CGO and YSZ form a solid solution at these temperatures by cation diffusion [8]. The $CGO_x : YSZ_{(1-x)}$ solid solution has a significantly lower oxide ion conductivity than either of the pure compounds [9–12], and thus may result in an increased cell resistance.

Interdiffusion barrier layers produced by screen-printing and spraying are generally of a thickness in the range 4–10 μm, although recent work by van Berkel et al. demonstrated screen-printed ceria barrier layers as thin as 1.4 μm [13]. However, the porosity of these screen-printed and sequentially fired barrier layers was in the range 25–30%, even after sintering at 1300 °C and it was shown that the ionic conductivity of the CGO layer was lower than expected due to interdiffusion between CGO and YSZ. An ideal bilayer electrolyte structure consisting of a 10 μm thick dense CGO layer on top of a 10 μm thick dense 8YSZ layer has approximately 26% greater resistance than the 8YSZ layer alone at 700 °C. Decreasing the thickness of the CGO layer to 1 μm reduces the bilayer resistance to a value only 2.6% greater than that of the 8YSZ layer alone [14,15].

By employing vacuum deposition techniques such as Chemical Vapour Deposition (CVD) [16], or different Physical Vapour Deposition (PVD) techniques such as Magnetron Sputtering [17], pulsed laser deposition [18], E-beam Evaporation [17], it is possible to pro-

* Corresponding author. Tel.: +45 4677 5807; fax: +45 4677 5858.
E-mail addresses: martin.soegaard@risoe.dk, msqg@risoe.dtu.dk (M. Søgaard).

0378-7753/$ – see front matter © 2010 Elsevier B.V. All rights reserved.
doi:10.1016/j.jpowsour.2010.08.108

duce very thin (submicrometer) and practically ideal barrier layers of CGO. However, scalability and cost-efficiency of these techniques are questionable for this application.

In this paper a reproducible way of producing a CGO barrier layer of nearly 100% volumetric density at temperatures below 1200 °C is presented, thus minimising detrimental interdiffusion between the YSZ electrolyte and the CGO barrier layer. Multiple spin-coating depositions of a solution containing the metal-nitrates, onto an anode supported YSZ electrolyte (a half-cell) in conjunction with a number of sintering steps were used to obtain dense and thin barrier layers.

2. Experimental

The spin-coated CGO layer was prepared by a so called 'wet route' using polymer precursors. The precursor was prepared by dissolving $Ce(NO_3)_3 \cdot 6H_2O$ and $Gd(NO_3)_3 \cdot 6H_2O$ (with molar ratio of Ce:Gd = 0.9:0.1) in ethylene glycol and water. In contrast to the procedures developed by Anderson et al. [19] no additional acids were added. The pH of the precursor solution was approximately neutral (pH ≈ 7) at all times.

The solution was stirred on a hot-plate in the temperature range 70–90 °C. Weighing after approximately 24 h of heating indicated that the water had completely evaporated. This state of the precursor will in the following be denoted as the initial state. When the initial state has been reached the ethylene glycol will start to evaporate and therefore the hot-plate temperature can be increased above 100 °C in order to speed up the preparation process of the precursor.

An important processing parameter is the viscosity of the precursor prior to spin-coating. The viscosity of the solution was measured as a function of time of heating to determine when the target viscosity (150 mPa s) was reached. A Haake Rheostress 600 controlled stress rate rheometer was used to collect viscosity data. Measurements were carried out under shear stress ranging from 0.02 to 12 Pa. A constant temperature of 21 °C was maintained for the experiment using a DC30 temperature control unit. Parallel plates with 60 mm diameter (PP60Ti) were used at a gap distance of 500 μm

The prepared solutions of polymer precursor were deposited on half-cells and spin coated. Several rotation rates were tested and finally a speed of 2000 round per minute (rpm) was chosen. If the rotation rate was significantly below 2000 rpm the deposited layer was too thick which was followed by formation of drying cracks. At rotation rates significantly above 2000 rpm a too small amount of precursor remained on the sample which caused dewetting of the CGO precursor solution. All results presented in the following are thus prepared at 2000 rpm. After spin-coating the layer was dried in a conveyor-belt furnace at 250 °C for 30 min except where noted. This procedure will be referred to as the 'deposition step' in the following.

The layer structure was investigated as a function of the number of deposition steps. After a certain number of deposition steps the layer was sintered at 1100 °C for 4 h. On the most promising samples with barrier layers a composite (50:50 wt%) LSCF:CGO cathode was deposited by screen printing and sintered at a temperature above 1000 °C. LSCF refers to $La_{0.58}Sr_{0.4}Co_{0.2}Fe_{0.8}O_{3-\delta}$ and CGO to $Ce_{0.9}Gd_{0.1}O_{1.95}$.

The crystal structure of the prepared layer was investigated with X-ray diffraction (XRD). A Stoe Bragg–Brentano X-ray diffractometer with Cu_{K_α} was used in the 2Θ range 15–90°. Reflections were collected with a rate of 0.6° per minute. The obtained diffraction patterns were compared with a prepared reference powder and with literature data.

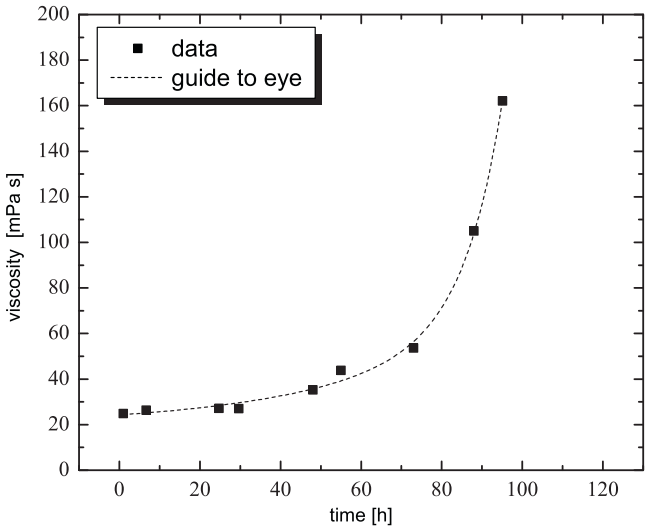

Fig. 1. Viscosity η of the precursor solution as a function of time. The line is a guide to the eye.

Scanning electron microscopy (SEM) was used to investigate the microstructure of the prepared layers. Images were taken using a Zeiss Supra 35 Field Emison SEM (FESEM) in standard and Inlense secondary electron imaging mode. Also, the back scatter electron detector was employed as to distinguish compositional differences. For cross section investigations samples were fractured or polished.

Thermogravimetry was used to study the thermal decomposition of the dried precursor using NETZSCH STA 409 PC/PG. The mass of the measured samples was 60.89 mg. The heating and cooling rates were 2 and 10 °C min^{-1}, respectively. The temperature range from 120 to 1150 °C was investigated.

Electrochemical impedance spectroscopy, EIS, measurements were carried out on the cell using a Solartron 1260 Gain-Phase Analyzer and in-house built cell voltage compensation electronics. The cell was sandwiched between ceramic gas distributor plates contacted by metal plates to give the following assembly: Ni-plate/Ni-YSZ cermet gas distributor plate/Fuel Cell/LSM gas distributor plate/Au-plate. This assembly was mounted in an alumina test house that was placed in a furnace. The test setup and alumina test house have been described in detail in Ref. [15]. The measurements described in this work were carried out at open circuit voltage (OCV) using a sinusoidal current perturbation with an RMS amplitude of 60 mA. All measurements were carried out with a total fuel flow of 25 l h^{-1} (26 ml min^{-1} cm^{-2}) and an oxidant flow of 140 l h^{-1} (146 ml min^{-1} cm^{-2}). The fuel was humidified hydrogen with 4% or 20% water, and the oxidant was air.

Polarisation curves were recorded in current controlled mode and the area specific secant resistance was determined at 0.6 V. The reported ASR values were corrected for fuel utilisation according to the procedure described in Ref. [20].

3. Results and discussion

From a previous study it is known that dense CGO layers can be produced using approximately 100 deposition steps [21]. In this article we investigate if it is possible to produce a similar layer in much fewer deposition steps. Three precursors with different viscosity were prepared to investigate the effect of layer production. Viscosities of 50, 100 and 150 mPa s were obtained by heating the initial solution. Viscosity as a function of time is shown in Fig. 1. It is observed that the precursor viscosity reach 50 mPa s after approximately 73 h. The target viscosities of 100 and 150 mPa s were obtained after 88 and 95 h, respectively. After reaching 100 mPa s

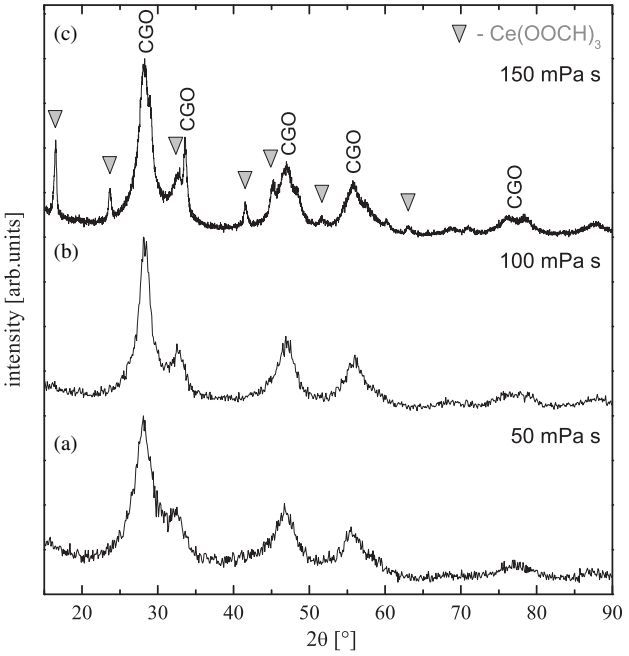

Fig. 2. XRD diffraction patterns of precursors of different viscosities dried at 130 °C for (a) 50 mPa s, (b) 100 mPa s and (c) 150 mPa s.

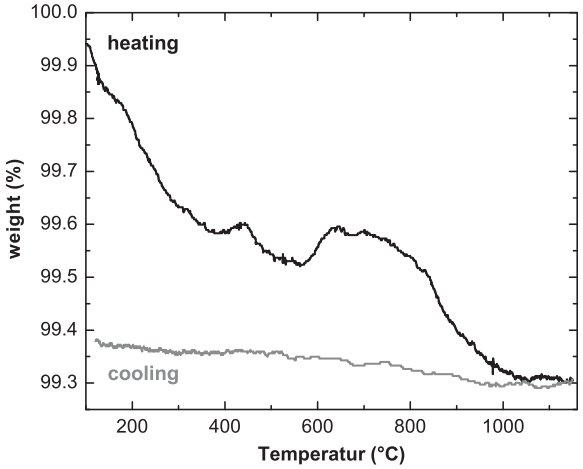

Fig. 3. The mass change of the powder as a function of temperature determined by the thermogravimetry. The powder was made from the polymer precursor of 50 mPa s dried at 130 °C.

the solution needs to be supervised carefully, as the viscosity starts to change rapidly. If the heat treatment is continued after reaching 150 mPa s a yellow precipitate will eventually form.

It was noticed that the precursor viscosity change is highly dependent on the evaporation area of the liquid, indicating that the viscosity rise, is due to a concentration change together with the proceeding polymerisation reaction [22,23]. During this reaction an intermediate product of cerium formate $Ce(OOCH)_3$ is formed. To confirm this, precursor solutions of different viscosity were dried at 130 °C in a furnace. This resulted in the formation of a powder for all three viscosities, which were investigated by XRD. The results are presented in Fig. 2. For the solution that had a viscosity of 100 mPa s the resulting powder shows traces of cerium formate. In the powder originating from the 150 mPa s viscous precursor, the formate phase is clearly identified. The most intensive peaks in all of three diffraction patterns originate from the CGO phase. From the width of the peak and Scherrer's equation the CGO particle size was calculated to 5 nm. A preliminary Transmission Electron Microscope (TEM) investigation also indicated the same particle size. From Rietveld refinement a cubic lattice parameter of $a = 5.4172$ Å was calculated. This value is consistent with literature (28795-ICSD).

The powder made of the precursor with the lowest viscosity was investigated using thermogravimetry (TG). Fig. 3 shows the weight loss as a function of temperature. The heat treatment at 250 °C used for drying the layers does not eliminate all the solvent remainings from the precursor. Continuous weight loss is observed up to 1000 °C. It is especially important to notice that the material continues to lose a significant amount of weight at temperatures above 800 °C. This indicates that the solvent remainings are present in the films even at very high temperatures and approximately 1000 °C is needed to obtain a pure layer containing only oxide. The mass increase observed between 600 and 800 °C is probably caused by material reoxidation after carbon burn out at 600 °C. Upon cooling no mass change within the uncertainty could be observed.

Following the results of Pan et al. [24] it should be possible to prepare a dense layer after 4–6 depositions using a 150 mPa s viscous precursor. In this study it was found that the 50 mPa s viscous precursor gave a better surface coverage during spin-coating deposition. The precursor with a viscosity of 150 mPa s was difficult to distribute homogeneously across the whole surface, resulting in an uneven layer formation. This could be due to the lower surface tension of the precursor with lower viscosity.

The precursors with different viscosities (50, 100, 150 mPa s) were deposited on half-cells in 2, 4 and 6 deposition steps. All samples were prepared using the same conditions and dried after every deposition in a conveyor belt furnace at 250 °C. From visual inspection it was observed that some samples were reflecting light which indicates a dense and crack-free surface. Samples where the surface looked frosted was attributed to a cracked layer. The surface of the prepared samples shows a layer that in most cases looks uniform, without visible large particles.

For cross section investigation samples were fractured and images were recorded using electron microscopy. Fig. 4 shows cross-sectional images of the deposited layers (heat treated at 250 °C). The seven images presented in Fig. 4 show the CGO layers produced at different precursor viscosities and number of deposition steps. The specific deposition conditions are provided in the figure caption.

It is observed that films could be produced using all three precursors and deposition steps. The films are porous and the thickness increase with the number of depositions. Only for the layer prepared from the precursor of 150 mPa s in six deposition steps a thickness exceeding 1 μm was obtained. All other prepared CGO layers were between 250 and 1000 nm thick. The thickness of the layer prepared from the 150 mPa s viscous precursor was not even along the sample surface and the continuity of the layer was broken in some parts of the deposited layers. The films produced with the 50 and the 100 mPa s viscous precursor have a uniform thickness and no discontinuities were observed. The sample prepared in six deposition steps from the 50 mPas s viscous precursor was selected for further investigations of the influence of the precursor remains on the sintering process. For this purpose the sample was fractured and pieces were individually sintered for 4 h at 600, 900 and 1100 °C.

The deposited and sintered layers were characterized using XRD, and the results are presented in Fig. 5. All collected diffraction patterns from the barrier layer deposition on half cells, showed peaks from YSZ (electrolyte), NiO (anode) and the layer of CGO. This is due to the penetration depth of the X-ray, that is grater than the thickness of the barrier layer and electrolyte. Even for the sintering temperature of 250 °C a CGO crystal structure can be identified. The grain sizes derived from the widening of the peaks using Scherrer's

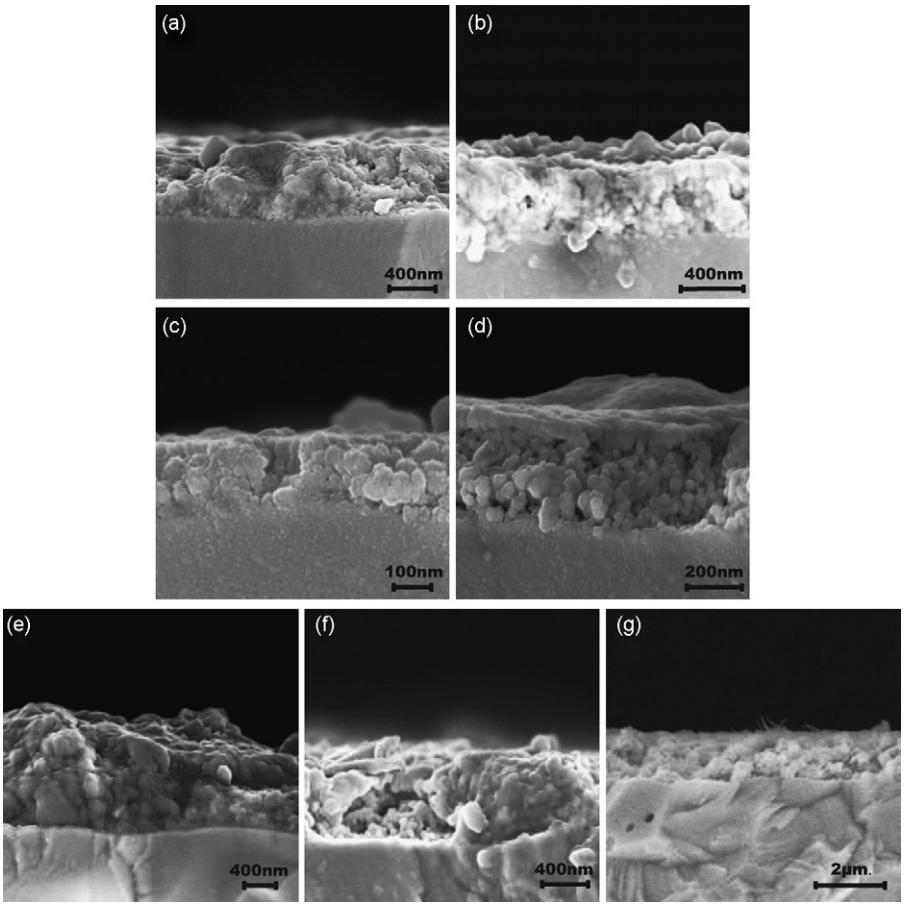

Fig. 4. Fracture cross section SEM pictures of prepared layers for (a) 4 depositions of 50 mPa s viscous precursor, (b) 6 depositions of 50 mPa s, (c) 2 depositions of 100 mPa s, (d) 4 depositions of 100 mPa s, (e) 2 depositions of 150 mPa s, (f) 4 depositions of 150 mPa s and (g) 6 depositions of 150 mPa s.

equation was estimated to 5, 9, 15 and 32 nm for 250, 600, 900 and 1100 °C, respectively. The increased intensity of the CGO peaks for the 900 °C samples is probably due to the crystallisation rate of the film.

Samples sintered at 900 and 1100 °C were polished and investigated by SEM. Fig. 6(a) shows a layer sintered at 900 °C and (b) at 1100 °C. For the film heat treated at 900 °C the sintering of the grains is causing the formation of many small closed porosities. For the sample sintered at 1100 °C it is observed that the grain coarsening is enhanced. The local densification of the layer caused by the merging of neighboring grains causes the closed porosity to become open. Because of this, a column like CGO structure is formed, with a spacing of around 20–50 nm between each column.

From Fig. 6 it is observed that the sintered CGO layers cannot be utilised as the interdiffusion barrier layer due to the open porosity. Therefore, it was investigated whether it is possible to refill the voids by further addition of CGO, i.e. that is to add further deposition steps after the porous layer has been formed. For this study 6 initial layers were deposited on a half-cell and sintered at 1100 °C. This was followed by two additional deposition steps that were sintered at 1100 °C. For both depositions steps the 50 mPa s viscous precursor was used. It is especially important for the deposition steps performed after the first high temperature sintering to use a low viscosity precursor, as this will facilitate the porosity infiltration. The resulting structure is shown in Fig. 7. A similar layer as for the 6 deposition steps is observed, however, at the interface region between CGO and YSZ electrolyte a thin dense structure can be seen. This dense structure is approximately 200 nm thick and join the initial columnar formations. No pin holes or porosity is observed in this layer.

This indicate that it is possible to fill the open porosity by increasing the number of deposition steps, corresponding to an increased amount of material infiltrating the pores. It should be noticed that the layer thickness after the initial 6 deposition steps is not increased, indicating that the material deposited in the following steps, infiltrate the porosity rather than sticking to the top of the layer. Based on these observations the following procedure was carried out in order to form a dense CGO layer: 4 deposition steps were performed and sintered at 1100 °C which form the initial CGO skeleton. To fill the open porosity in the created structure, 10 deposition steps were performed and sintered at 1100 °C. This was followed by additional 6 deposition steps and sintering at 1100 °C. The third deposition round was performed in order to close the porosity created in the second deposition round. The resulting layer is shown in Fig. 8.

It is observed that even after sintering at 1100 °C the CGO layer remains dense with no visible cracks or holes. The layer thickness is in general very even, with a thickness of 1.5 μm along the whole sample surface. Several samples were prepared using the described procedure and all of them gave a similar microstructure.

The above procedure was used to prepare a CGO interdiffusion barrier layer on 53 mm × 53 mm half-cells, which was followed by screen printing of a composite $(La,Sr)(Fe,Co)O_{3-\delta}$:$Ce_{0.9}Gd_{0.1}O_{1.95}$ cathode. The last CGO deposition round was co-sintered with the cathode at a temperature below 1100 °C. Fig. 9 shows a back scatter SEM image of a polished cross-section of the prepared fuel cell. It is observed that the CGO layer has a thickness approximately 1 μm and does not delaminate either from the electrolyte ynor from the cathode. The CGO layer prepared together with the cathode seems to be even more dense than previously, which is probably related

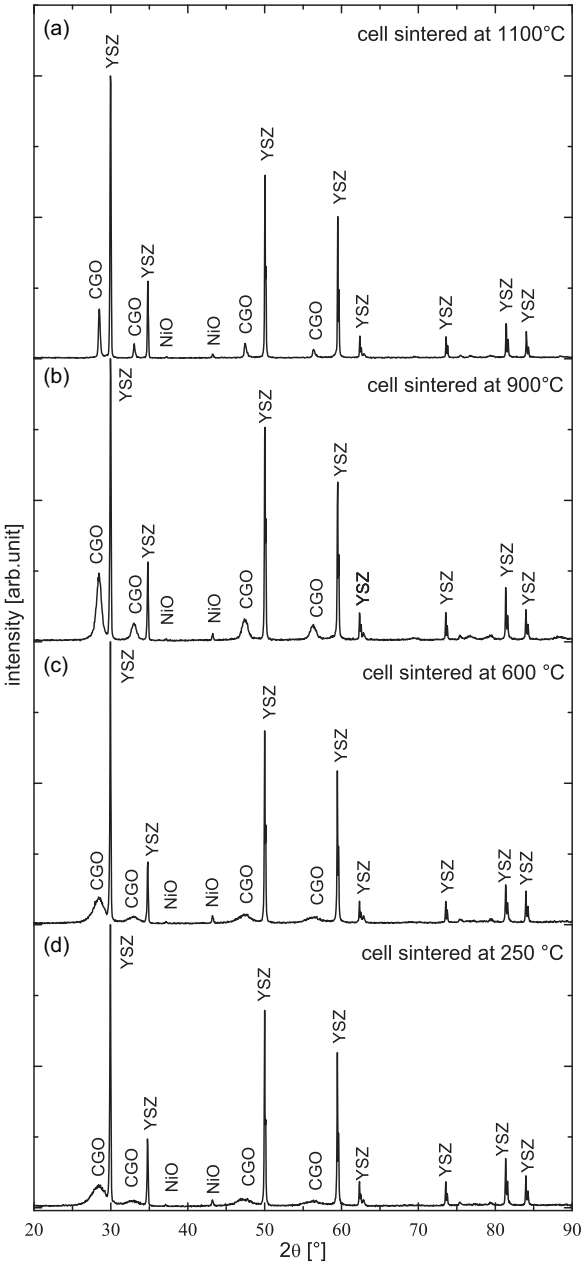

Fig. 5. XRD patterns of the CGO layers sintered at three different temperatures (a) 900 °C, (b) 600 °C and (c) 250 °C

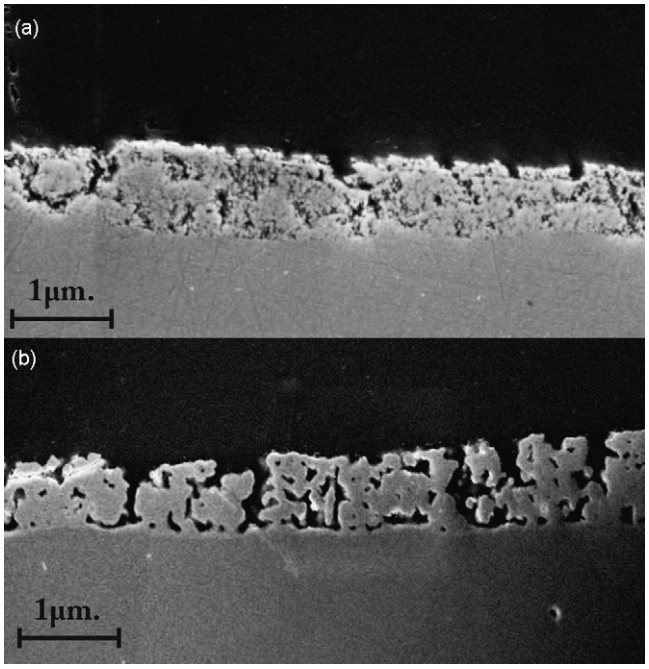

Fig. 6. SEM images of polished samples where the CGO layers have been sintered at (a) 900 °C and (b) 1100 °C

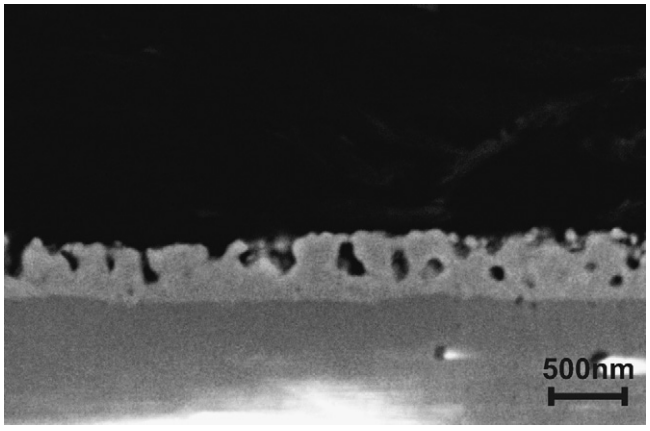

Fig. 7. SEM pictures of CGO after 6 depositions steps sintered at 1100 °C followed by 2 depositions sintered at 1100 °C.

to the presence of sintering agents, i.e. cobalt [25]. Based on the methods used in this study, no additional phases were identified at the interface between the barrier layer and the electrolyte. However, in Fig. 9 the slight change of the YSZ colour at the interface can indicate the formation of thin a zirconate layer.

Two cells with approximately 1 µm thick barrier layers, and screen-printed LSCF:CGO cathodes were selected and electrochemically tested. The cell performance was measured using ac and dc techniques in the temperature range 850–650 °C. In order to gauge the resistance of the bilayer (CGO–YSZ) electrolyte the serial resistance of the cells was determined by electrochemical impedance spectroscopy. In the absence of current constriction and significant contact resistances the serial resistance of the cell corresponds to the resistance contribution from the (bilayer) electrolyte. In this case the serial resistance of two cells with spin-coated barrier layers was compared to that of four cells with nominally identical cathodes and half-cells, but with sprayed and co-fired barrier layers of

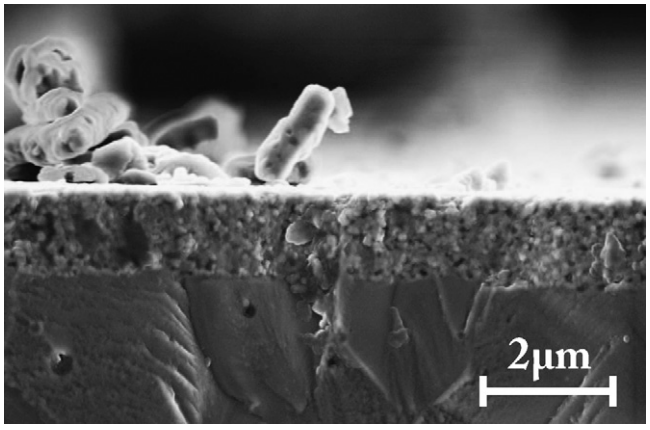

Fig. 8. SEM image of layer prepared in several deposition steps (fractured surface).

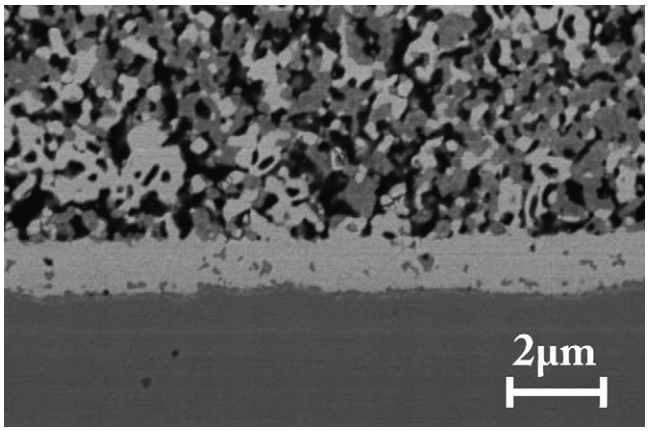

Fig. 9. SEM image of the layer prepared in several deposition steps (polished surface).

significantly greater porosity, or barrier layers produced by pulsed laser deposition (PLD), see Fig. 10.

The data in Fig. 10 clearly shows that the total bilayer resistance is smaller for the spin-coated barrier layers, than for the sprayed and co-fired barrier layer, but somewhat greater than for the layers deposited by PLD. Examples of polarisation curves recorded for cells with three different barrier layers are displayed in Fig. 11. The performance reduction of the cell with the spin-coated barrier layer is most likely due to a small amount of zirconate formed at the CGO/YSZ interface. It was reported in the literature [26,27] that the migration of the strontium can occur not only through the voids in the barrier layer but also through the grain boundaries of the CGO. The grain size of the layers produced in this study is smaller than the one obtained from PLD. This translates into a significantly greater amount of grain boundaries in the CGO layer deposited by spin-coating, as compared to a barrier layer produced by PLD [26], which may result in a slightly increased rate of zirconate formation at the barrier–electrolyte interface. However, the investigation of the samples without the barrier layer indicates that an insulating layer of approximately 1 μm is formed during the cathode sintering process. Using the literature data the resistance of such interlayer was estimated to be more than three times higher than the R_S measured in this study (i.e. approximately 0.6 Ω cm^2 at 750 °C) [4]. The

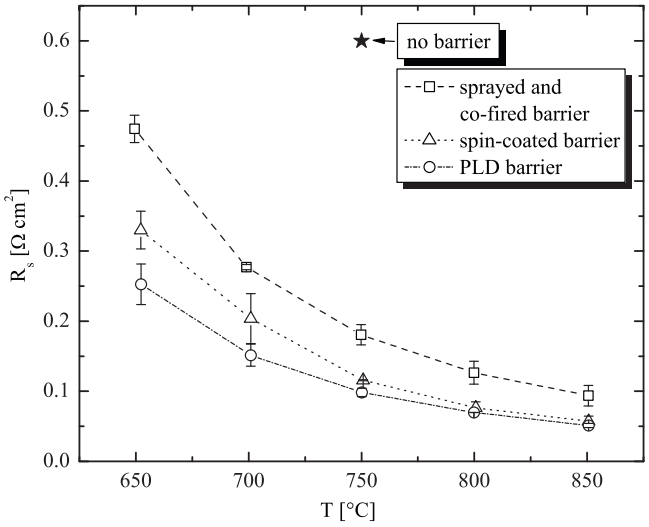

Fig. 10. Measured serial resistance of six cells with three different barrier layers as a function of operating temperature. The error bars represent the confidence interval at the 95 % level.

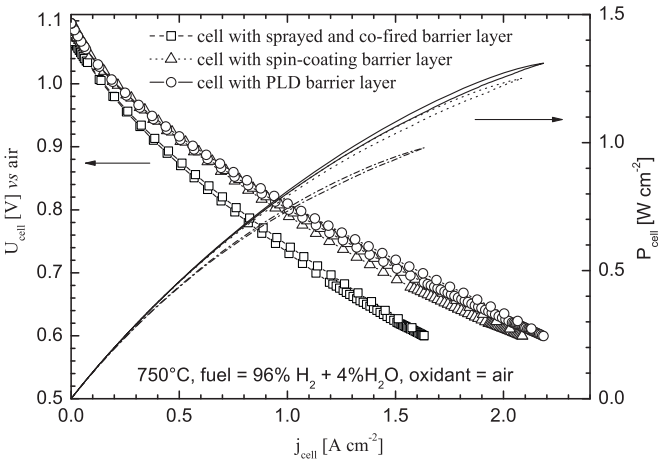

Fig. 11. DC polarisation curves (and power curves) recorded at 750 °C for a cells with three different barrier layers.

Table 1
The Area Specific Resistance (ASR) and serial resistance R_S for cells with different barrier layers measured at 750 °C.

Barrier layer on cell	T_{cell} (at OCV) [°C]	ASR at 0.6 V [Ω cm^2]	R_S (at OCV) [Ω cm^2]
Sprayed and co-fired	750	0.26 (±0.04)	0.18 (±0.02)
Spin-coated	750	0.18 (±0.01)	0.11 (±0.01)
PLD	750	0.18 (±0.01)	0.10 (±0.01)

estimated resistance is plotted in Fig. 10 for comparison. A summary of the performance of the cells with the three different barrier layers is presented in Table 1. The lower resistance recorded with the presence of the spin-coated CGO barrier clearly indicates that the formation of insulating layer was significantly reduced.

4. Conclusions

A method for producing a barrier layer of CGO was developed using spin coating. The described spin coated barrier layer was evaluated using an anode supported cell with a $La_{0.58}Sr_{0.4}Fe_{0.8}Co_{0.2}O_3$:$Ce_{0.9}Gd_{0.1}O_{1.95}$ cathode. The thin CGO layer was sufficient to prevent reactions between the perovskite based electrode and the YSZ electrolyte on cathode firing. Further, no solid solution formation between the YSZ and CGO layer could be observed using electron microscopy. The electrochemical performance of the cell was evaluated using impedance spectroscopy and from this a series resistance could be deduced. This series resistance was significantly lower than a similar cell (same half-cell and cathode) employing a sprayed and co-fired CGO barrier layer. The series resistance was slightly higher than a cell with a barrier layer produced using pulsed laser deposition. In conclusion an easy upscalable method for the deposition of a thin CGO layer using spin coating on an already sintered anode supported YSZ-electrolyte was demonstrated.

Acknowledgement

The testing work that we carried out for this paper was part of our effort within SOFC600 (SES-2006-020089), which needs to be acknowledged.

References

[1] A. Weber, E. Ivers-Tiffee, Journal of Power Sources 127 (2004) 273–283.
[2] G.C. Kostogloudis, C. Ftikos, Journal of the European Ceramic Society 18 (1998) 1707–1710.

[3] S. Simner, J. Shelton, M. Anderson, J. Stevenson, Solid State Ionics 161 (2003) 11–18.
[4] F.W. Poulsen, N. van der Puil, Solid State Ionics 53–56 (1992) 777–783.
[5] T. Ishihara, N.M. Sammes, O. Yamamoto, High Temperature Solid Oxide Fuel Cells – Fundamentals, Design and Applications, Elsevier Ltd., Oxford, UK, 2003.
[6] L. Rose, M. Menon, K. Kammer, O. Kesler, P.H. Larsen, Advanced Materials Research 15–17 (2006) 293–298.
[7] K.K. Hansen, M. Menon, J. Knudsen, N. Bonanos, M. Mogensen, Journal of The Electrochemical Society 157 (3) (2010) B309–B313.
[8] A. Mai, V.A. Haanappel, F. Tietz, D. Stöver, Solid State Ionics 177 (2006) 2103–2107.
[9] A. Tsoga, A. Naoumidis, D. Stöver, Solid State Ionics 135 (2000) 403–409.
[10] A. Tsoga, A. Gupta, A. Naoumidis, P. Nikolopoulos, Acta Materialia 48 (2000) 4709–4714.
[11] J. Bentzen, H. Schwartzbach, Solid State Ionics 40–41 (1990) 942.
[12] N. Sammes, G. Tompsett, Z. Cai, Solid State Ionics 121 (1999) 121.
[13] F.P.F. van Berkel, Y. Zhang-Steenwinkel, G.P.J. Schoemakers, M.M.A. van Tuel, G. Rietveld, ECS Transactions 25 (2) (2009) 2717.
[14] M. Mogensen, D. Lybye, K. Kammer, N. Bonanos, ECS Meeting Abstracts 501 (2006) 1136–11136.
[15] C.C. Appel, N. Bonanos, A. Horsewell, S. Linderoth, Journal of Materials Science 36 (2001) 4493–4501.
[16] K.K. Schuegraf, Handbook of Thin Film Deposition Processes and Techniques (Materials and Processing Technology), William Andrew, 2002.
[17] D.L. Smith, Thin-Film Deposition: Principles & Practice, McGraw-Hill Professional, 1995, ISBN 0–07-058502–4.
[18] D. Chrisey, G. Hubler, Pulsed Laser Deposition of Thin Films, John Wiley & Sons, Inc., 1994.
[19] I. Kosacki, T. Suzuki, V. Petrovsky, H. Anderson, Solid State Ionics 136–137 (2000) 1225–1233.
[20] M. Mogensen, P.V. Hendriksen, High temperature Solid Oxide Fuel Cells – Fundamentals, Design and Applications, Elsevier Ltd., Oxford, UK, 2003.
[21] P. Plonczak, M. Gazda, B. Kusz, P. Jasinski, Journal of Power Sources 181 (2008) 1–7.
[22] C. Ho, J. Yu, T. Kwong, A. Mak, S. Lai, Chemistry of Materials 17 (2005) 4514–4522.
[23] R. Turcotte, J. Haschke, M. Jenkins, L. Eyring, Journal of Solid State Chemistry 2 (1970) 593–602.
[24] Y. Pan, J.H. Zhu, M.Z. Hu, E. Payzant, Surface & Coating Technology 200 (2005) 1242–1247.
[25] Z. Wang, S. ichi Hashimoto, M. Mori, Journal of Power Sources 193 (2009) 49–54.
[26] R. Knibbe, J. Hjelm, M. Menon, N. Pryds, M. Søgaard, H.J. Wang, K. Neufeld, Journal of the American Ceramic Society (2010) 1–7.
[27] N. Sakai, H. Kishimoto, K. Yamaji, T. Horita, M. Brito, H. Yokokawa, ECS Transactions 7 (2007) 389–398.